



UvA-DARE (Digital Academic Repository)

Constraints on decaying dark matter from the extragalactic gamma-ray background

Ando, S.; Ishiwata, K.

DOI

[10.1088/1475-7516/2015/05/024](https://doi.org/10.1088/1475-7516/2015/05/024)

Publication date

2015

Document Version

Author accepted manuscript

Published in

Journal of Cosmology and Astroparticle Physics

[Link to publication](#)

Citation for published version (APA):

Ando, S., & Ishiwata, K. (2015). Constraints on decaying dark matter from the extragalactic gamma-ray background. *Journal of Cosmology and Astroparticle Physics*, 2015(5), [024]. <https://doi.org/10.1088/1475-7516/2015/05/024>

General rights

It is not permitted to download or to forward/distribute the text or part of it without the consent of the author(s) and/or copyright holder(s), other than for strictly personal, individual use, unless the work is under an open content license (like Creative Commons).

Disclaimer/Complaints regulations

If you believe that digital publication of certain material infringes any of your rights or (privacy) interests, please let the Library know, stating your reasons. In case of a legitimate complaint, the Library will make the material inaccessible and/or remove it from the website. Please Ask the Library: <https://uba.uva.nl/en/contact>, or a letter to: Library of the University of Amsterdam, Secretariat, Singel 425, 1012 WP Amsterdam, The Netherlands. You will be contacted as soon as possible.

UvA-DARE is a service provided by the library of the University of Amsterdam (<https://dare.uva.nl>)

Constraints on decaying dark matter from the extragalactic gamma-ray background

Shin'ichiro Ando^a and Koji Ishiwata^b

^aGRAPPA Institute, University of Amsterdam, 1098 XH Amsterdam, The Netherlands

^bDeutsches Elektronen-Synchrotron DESY, Notkestrasse 85, 22607 Hamburg, Germany

E-mail: s.ando@uva.nl, koji.ishiwata@desy.de

Abstract. If dark matter is unstable and the mass is within GeV–TeV regime, its decays produce high-energy photons that give contribution to the extragalactic gamma-ray background (EGRB). We constrain dark matter decay by analyzing the 50-month EGRB data measured with Fermi satellite, for different decay channels motivated with several supersymmetric scenarios featuring R -parity violation. We adopt the latest astrophysical models for various source classes such as active galactic nuclei and star-forming galaxies, and take associated uncertainties properly into account. The lower limits for the lifetime are very stringent for a wide range of dark matter mass, excluding the lifetime shorter than 10^{28} s for mass between a few hundred GeV and ~ 1 TeV, e.g., for $b\bar{b}$ decay channel. Furthermore, most dark matter models that explain the anomalous positron excess are also excluded. These constraints are robust, being little dependent on astrophysical uncertainties, unlike other probes such as Galactic positrons or anti-protons.

Contents

1	Introduction	1
2	Decaying dark matter	3
2.1	Formulation	3
2.2	Dark matter models	4
2.2.1	Wino	4
2.2.2	Sneutrino	5
2.2.3	Gravitino	6
2.2.4	Axino	6
2.3	Gamma-ray fluxes (examples)	7
3	Astrophysical source	8
3.1	Blazars	8
3.2	Star-forming galaxies	9
3.3	Misaligned active galactic nuclei	9
4	Results	9
4.1	Analysis	10
4.2	Constraints on dark matter lifetime	11
4.3	Implications for particle physics models	14
5	Discussion	15
5.1	Comparison with constraints from galaxy clusters and dwarf galaxies	15
5.2	Comparison with constraints from Galactic anti-protons	16
6	Conclusions	16

1 Introduction

Recent cosmological measurements of the cosmic microwave background (CMB) [1, 2] conclusively show that about 84% of matter in the Universe is made of dark matter. Evidently these dark matter particles are electromagnetically neutral and also stable compared to cosmological time scale. However, it does not necessarily mean that they have infinite lifetime. In most cases, dark matter is simply assumed to be stable, e.g., by introducing Z_2 symmetry in the Lagrangian. One of the most popular examples of such symmetries is R -parity in supersymmetric models, which is often introduced to make protons stable. It also stabilizes the lightest superparticle (LSP) to be a candidate for dark matter. However, whether dark matter is absolutely stable or not, and hence whether such symmetry as R -parity exists or is broken, should be tested in light of modern data.

Dark matter decays produce cosmic ray particles, and details of the final state depends on its interaction with standard-model particles. In supersymmetry, R -parity violation (RPV) allows the LSP to decay to standard-model particles, and this is indeed favorable for some supersymmetric scenarios from cosmology arguments. For instance, if gravitino, a superpartner of the graviton, is the LSP, the next-LSP may decay during big-bang nucleosynthesis, which destroys light elements. In RPV scenario, however, the gravitino dark

matter with mass of order 0.1–1 TeV makes it possible to overcome such cosmological problem [3]. For gravitino dark matter models, it was pointed out that the decay channels of gauge/Higgs bosons plus lepton dominate the total decay width under bi-linear RPV, which can produce observable high energy hadrons and leptons [4]. Another possibility is axino — a superpartner of axion, which in some supersymmetric scenarios becomes the LSP [5–10] and plays the role of dark matter [11–13] (see also Refs. [14, 15] for cosmology of supersymmetric axion model). Recently Ref. [16, 17] studied the axino dark matter with RPV in order to explain the observed baryon asymmetry. In this case RPV is crucial for baryogenesis, which is directly connected to hadronic products in axino decay.¹ Finally, anomalous cosmic ray positron fraction observed with PAMELA [19, 20], Fermi [21] and AMS-02 [22, 23] motivated intensive (in many cases phenomenological) discussions on leptophilic models, where dark matter particles decay (or annihilate) mainly into multiple leptons.

In this paper, we study the impact of dark matter decays on the latest gamma-ray observations with the Large Area Telescope (LAT) onboard the Fermi satellite. In order to obtain stringent, yet robust, constraints, we adopt the latest data for the extragalactic gamma-ray background (EGRB) [24], which is isotropic gamma-ray radiation from every direction of the sky. Strictly speaking, EGRB is approximately isotropic since it partly consists of gamma rays from point sources (we will see in detail later). However, it is a good approximation to say that EGRB is isotropic statistically. Since we compare the EGRB data with the contribution from dark matter decays that is the *statistical average* of gamma-ray radiation from each of dark matter structures, this yields results that are largely independent of any uncertain inputs such as density profiles of dark matter halos. In addition, we take into account secondary gamma rays due to the inverse Compton (IC) scattering by the charged particles from decays off the CMB photons as discussed in Ref. [25].² This again yields no theoretical uncertainties if a decaying dark matter model is specified; we do not include any other seed photons such as regular optical emission from galaxies. It is also known that hadronic decay of dark matter is strictly constrained by measurements of cosmic ray anti-protons [27–31]. Besides the fact that these anti-proton constraints are subject to much larger uncertainties due to Galactic cosmic ray propagation, we will show that the latest EGRB measurement gives more stringent constraints at this point. This should of course be revisited after the release of AMS-02 data for anti-protons and other light elements.

Compared with the earlier work (see, e.g., Refs. [32, 33] and references therein) based on the Fermi-LAT EGRB data collected for 10 months [34], we improve upon the following points. Firstly, we adopt the latest EGRB data measured with Fermi-LAT for 50 months [24].³ Secondly, we address the systematic uncertainties that come from the modeling and subtraction of the Galactic foreground emission, and find that they reflect on uncertainties for lifetime constraints by a factor of a few. Lastly, in addition to purely phenomenological power-law modeling of other components, we use more realistic astrophysical components modeled individually with latest gamma-ray luminosity functions calibrated with other wavebands. We also adopt the uncertainties associated with these modeling as prior information in Bayesian statistical analyses to obtain lifetime constraints of dark matter. It is found that the obtained lower limit on the decay lifetime is improved by about an order of magnitude compared with Ref. [32], for all the hadronic and leptonic decay channels. For example, for a conventional model of decays into $b\bar{b}$, we find that the lifetime shorter than

¹This is an explicit realization of the baryogenesis, which is proposed in Ref. [18].

²IC photon in annihilating dark matter is studied in Ref. [26].

³Constraint on annihilating dark matter in light of the 50-month data is studied in Refs. [35–37].

10^{28} s is excluded for dark matter masses between a few 100 GeV to 1 TeV. In addition, it is found that the parameter space which is motivated to explain the positron excess is almost excluded.

This paper is organized as follows. In Sec. 2, we give formulation of the EGRB computation from dark matter decays, and several models that give finite lifetime to dark matter. Section 3 then discusses three astrophysical components that are considered for the analysis. Results are presented in Sec. 4 along with details of the analysis, and we discuss several important implications in Sec. 5. Throughout this paper, we use cosmological parameters given by Planck collaboration combined with WMAP [2]: present Hubble rate, and density divided by critical density of matter, dark matter, dark energy are $H_0 = 67.04 \text{ km s}^{-1} \text{ Mpc}^{-1}$ (i.e., $h = 0.6704$), $\Omega_m = 0.3183$, $\Omega_{\text{dm}} = 0.2678$, $\Omega_\Lambda = 0.6817$, respectively. The critical density is obtained by $\rho_c = 1.054 \times 10^{-5} h^2 \text{ GeV cm}^{-3}$.

2 Decaying dark matter

Gamma rays from decaying dark matter is determined with three ingredients: dark matter mass, lifetime, and energy distribution of particles per decay, i.e.,

$$m_{\text{dm}}, \tau_{\text{dm}}, \frac{dN_I}{dE} \quad (I = \gamma, e^\pm, \dots), \quad (2.1)$$

where the subscript ‘dm’ stands for dark matter. First two are free parameters, while the dN_I/dE is computed for each dark matter model. We formulate the EGRB from decaying dark matter based on Refs. [4, 25], then discuss dark matter models on which we focus.

2.1 Formulation

Dark matter contribution to the EGRB consists of two components: primary and secondary gamma rays. Secondary gamma rays are produced by IC scattering off the CMB photons due to electrons and positrons from dark matter decay. The total gamma-ray intensity $\Phi_\gamma^{\text{dm}}(E_\gamma)$ is expressed as

$$\Phi_\gamma^{\text{dm}}(E_\gamma) = \frac{c}{4\pi} \frac{\Omega_{\text{dm}} \rho_c}{m_{\text{dm}} \tau_{\text{dm}}} \int dt Q_\gamma^{\text{dm}}(E_\gamma, E'_\gamma), \quad (2.2)$$

where c is speed of light, t is cosmic time, $E'_\gamma = (1+z)E_\gamma$ is the energy of γ -rays when they are produced at redshift z , and

$$Q_\gamma^{\text{dm}}(E_\gamma, E'_\gamma) = e^{-\tau(z, E_\gamma)} (1+z) [\mathcal{P}_{\text{prim}}(E'_\gamma) + \mathcal{P}_{\text{ic}}(E'_\gamma)], \quad (2.3)$$

where $\tau(z, E_\gamma)$ is optical depth, which we adopt the result given in Ref. [38]. $\mathcal{P}_{\text{prim}}(E'_\gamma)$ and $\mathcal{P}_{\text{ic}}(E'_\gamma)$ are energy distributions of primary and IC γ -rays, which are given by

$$\mathcal{P}_{\text{prim}}(E'_\gamma) = \frac{dN_\gamma}{dE}(E'_\gamma), \quad (2.4)$$

$$\mathcal{P}_{\text{ic}}(E'_\gamma) = \frac{c}{1+z} \int dE_e dE_{\gamma\text{CMB}} \frac{d\sigma_{\text{IC}}}{dE'_\gamma}(E'_\gamma, E_e, E_{\gamma\text{CMB}}) f_{\text{CMB}}(E_{\gamma\text{CMB}}) \frac{Y_e(E_e)}{b_{\text{ic}}(E_e)}, \quad (2.5)$$

respectively, where $d\sigma_{\text{IC}}/dE'_\gamma$ is the differential cross section of the IC process, f_{CMB} is the spectrum of the CMB (per unit volume per unit energy), and $b_{\text{ic}} = (4/3)\sigma_{\text{T}}(E_e/m_e)^2 \rho_{\text{CMB}}^{(\text{now})}$

is the energy loss rate of the e^\pm due to the IC process. Here σ_T is Thomson scattering cross section and $\rho_{\text{CMB}}^{(\text{now})} \simeq 0.260 \text{ eV cm}^{-3}$, and $Y_e(E_e)$ is defined by using dN_{e^\pm}/dE as

$$Y_e(E_e) = \int_{E_e}^{\infty} dE \left[\frac{dN_{e^+}}{dE}(E) + \frac{dN_{e^-}}{dE}(E) \right]. \quad (2.6)$$

Then after changing variable from t to E'_γ , it is straightforward to obtain

$$\begin{aligned} E_\gamma^2 \Phi_\gamma^{\text{dm}}(E_\gamma) &= \frac{c}{4\pi} \frac{\Omega_{\text{dm}} \rho_c}{m_{\text{dm}} \tau_{\text{dm}}} \frac{E_\gamma}{H_0} \int_{E_\gamma}^{\infty} dE'_\gamma \frac{E_\gamma}{E'_\gamma} \frac{Q_\gamma^{\text{dm}}(E_\gamma, E'_\gamma)}{\sqrt{\Omega_\Lambda + \Omega_m(E'_\gamma/E_\gamma)^3}} \\ &= 1.4 \times 10^{-7} \text{ GeV cm}^{-2} \text{ s}^{-1} \text{ sr}^{-1} \left(\frac{1 \text{ TeV}}{m_{\text{dm}}} \right) \left(\frac{10^{27} \text{ s}}{\tau_{\text{dm}}} \right) \left(\frac{E_\gamma}{100 \text{ GeV}} \right) \\ &\times \int_{E_\gamma}^{\infty} dE'_\gamma \frac{E_\gamma}{E'_\gamma} \frac{Q_\gamma^{\text{dm}}(E_\gamma, E'_\gamma)}{\sqrt{\Omega_\Lambda + \Omega_m(E'_\gamma/E_\gamma)^3}}. \end{aligned} \quad (2.7)$$

2.2 Dark matter models

Decaying dark matter models can be classified into three categories by the products after cascade decay: (i) lepton, (ii) hadron + lepton and (iii) hadron. Decaying dark matter models of class (i) and (ii) are particularly popular since energetic positron due to the decay can account for the cosmic-ray positron excess which was reported by PAMELA [19, 20], Fermi-LAT [21] and AMS-02 [22, 23], with a proper choice of τ_{dm} and m_{dm} . To do comprehensive analysis, we consider several dark matter models in supersymmetric theory and compute gamma-ray distribution for each case.

In supersymmetric models, the LSP becomes unstable once RPV operators are introduced in the superpotential,

$$W_{\hat{R}_p} = \mu_i \hat{L}_i \hat{H}_u + \lambda_{ijk} \hat{Q}_i \hat{L}_j \hat{D}_k^c + \lambda'_{ijk} \hat{L}_i \hat{L}_j \hat{E}_k^c + \lambda''_{ijk} \hat{U}_i \hat{D}_j^c \hat{D}_k^c, \quad (2.8)$$

where i, j, k are generation indices, \hat{Q}_i (\hat{L}_i) is left-handed quark (lepton), \hat{U}_i^c , \hat{D}_i^c (\hat{E}_i^c) are right-handed up- and down-type quarks (lepton), and \hat{H}_u is up-type Higgs. We use ‘hat’ to represent chiral superfields (superpartners are expressed by using ‘tilde’ in the later discussion). The final state of dark matter decay depends on which of the above RPV interaction terms are operative. For the purpose mentioned above, we consider wino, sneutrino, gravitino and axino as the LSP. Simulated gamma-ray fluxes are summarized in Fig. 1, for which we will give the details below.

2.2.1 Wino

Winos are superpartner of W bosons. In a wide range of anomaly-mediated supersymmetry breaking scenario [39], neutral wino \tilde{W}^0 is the LSP and it is a viable candidate for dark matter with a mass of a few hundred GeV [40] or around 3 TeV [41]. Besides, scalar partners of quarks/leptons are much heavier than TeV scale in anomaly mediation, which is consistent with 126 GeV Higgs boson discovered at the LHC [42, 43]. Testing wino dark matter is pointed out to be promising in direct [44] or indirect [45] detection experiments. More recently cosmic rays from decaying wino is studied in LLE^c RPV [46] to explain the latest cosmic-ray positron excess reported in AMS-02 [22, 23]. We study the same type of RPV considered in Ref. [46] to simulate gamma ray.

Since squarks are much heavier than winos, it is instructive to write down interactions of \tilde{W}^0 which are relevant for the decay in higher dimension operators. In large slepton limit, they are given by

$$\mathcal{L}_{\text{int}} = \frac{\lambda'_{ijk}}{\Lambda^2} \left[(\tilde{W}^0 P_L e_j)(\bar{e}_k P_L \nu_j) + (\tilde{W}^0 P_L \nu_j)(\bar{e}_k P_L e_j) \right] + \text{h.c.} \quad (2.9)$$

where $P_L = (1 - \gamma_5)/2$, $1/\Lambda^2 = \sqrt{2}g_2/m_{\tilde{L}_j}^2$, and summation of flavor index should be taken for $i < j$. g_2 is $SU(2)_L$ gauge coupling constant and $m_{\tilde{L}_j}$ is soft supersymmetry breaking mass for left-handed slepton. We have assumed $m_{\tilde{L}_j} < m_{\tilde{L}_i}$ for $i < j$. Wino decay as $\tilde{W}^0 \rightarrow \nu_i e_j^- e_k^+$ ($\bar{\nu}_i e_j^+ e_k^-$) and $\nu_j e_i^- e_k^+$ ($\bar{\nu}_j e_i^+ e_k^-$). If lepton masses are ignored, then the energy distribution of final state leptons is simply given by

$$\frac{d^2\Gamma_{\tilde{W}^0 \rightarrow \nu_i e_j^- e_k^+}}{dz_j dz_k} = \frac{d^2\Gamma_{\tilde{W}^0 \rightarrow \bar{\nu}_i e_j^+ e_k^-}}{dz_j dz_k} = \frac{|\lambda'_{ijk}|^2 m_{\tilde{W}^0}^5}{512\pi^3 \Lambda^4} z_j(1 - z_j), \quad (2.10)$$

$$\frac{d^2\Gamma_{\tilde{W}^0 \rightarrow \nu_j e_i^- e_k^+}}{dz_i dz_k} = \frac{d^2\Gamma_{\tilde{W}^0 \rightarrow \bar{\nu}_j e_i^+ e_k^-}}{dz_i dz_k} = \frac{|\lambda'_{ijk}|^2 m_{\tilde{W}^0}^5}{512\pi^3 \Lambda^4} z_j(1 - z_j), \quad (2.11)$$

where $m_{\tilde{W}^0}$ is wino mass and $z_\alpha = 2E_\alpha/m_{\tilde{W}^0}$ ($\alpha = i, j, k$) are defined by the energy E_α of ν_i, e_j^-, e_k^+ and so on. They satisfy $z_i + z_j + z_k = 2$ and $0 \leq z_{i,j,k} \leq 1$ (see also Ref. [47]). Then the energy distribution for charged leptons in the final state is given by

$$\frac{dN_{e_j}}{dz_{e_j}} = 12z_{e_j}^2(1 - z_{e_j}), \quad \frac{dN_{e_k}}{dz_{e_k}} = 2z_{e_k}^2(3 - 2z_{e_k}), \quad (2.12)$$

in a single process $\tilde{W}^0 \rightarrow \nu_i e_j^- e_k^+$, and

$$\frac{dN_{e_\beta}}{dz_{e_\beta}} = 2z_{e_\beta}^2(3 - 2z_{e_\beta}), \quad (2.13)$$

where $\beta = i, k$ in $\tilde{W}^0 \rightarrow \nu_j e_i^- e_k^+$. Energy distribution for each particle in CP conjugated final state is the same as in original state. For example, if λ_{122} is only relevant, then the final state in wino decay is $\nu_e \mu^- \mu^+$ ($\bar{\nu}_e \mu^+ \mu^-$) and $\nu_\mu e^- \mu^+$ ($\bar{\nu}_\mu e^+ \mu^-$). Thus no primary gamma rays or (anti-)protons are generated. In such case, IC photons from e^\pm (which includes electron and positron from μ^\pm) are the only observable gamma rays. If τ^\pm is produced, then its cascade decay produce energetic gamma rays. We use PYTHIA [48] to compute dN_I/dE ($I = \gamma, e^\pm$) in the primary decay of dark matter.

2.2.2 Sneutrino

As a reference, we also consider right-handed sneutrino dark matter in LLE^c RPV. Supposing that neutrinos are purely-Dirac fermions, neutrino Yukawa couplings are very small, i.e. $\mathcal{O}(10^{-13})$. Since right-handed sneutrinos, superpartners of right-handed neutrinos, interact with the other particles via the Yukawa couplings, the lightest one can be dark matter if it is the LSP [49]. In LLE^c type RPV, right-handed sneutrino $\tilde{\nu}_{Ri}$ decays to charged leptons $l_j^+ l_k^-$. We will compute gamma-ray flux for the final state $l_j^+ l_k^-$.⁴

⁴Electroweak correction to the final state becomes important when dark matter mass is extremely large. However, we have checked numerically that it does not affect the result when the mass is less than 10 TeV.

2.2.3 Gravitino

In R -parity conserved case, gravitino LSP is typically disfavored in cosmology when it has electroweak-scale mass. This is because the next-LSP (NLSP), which is usually the LSP in the minimal supersymmetric standard model and decays to gravitino and standard-model particles via Planck-suppressed interaction, becomes long-lived and may decay after big-bang nucleosynthesis (BBN) started. In the RPV case, however, NLSP can decay to standard-model particles via RPV interaction before BBN starts. Thus NLSP decay does not affect BBN. Furthermore, gravitino is cosmologically long-lived since the decay rate is suppressed by the Planck mass and a small violation of R -parity, thus it can play the role of dark matter [3]. In bi-linear RPV, for example, gravitino $\psi_{3/2}$ decays to $\gamma\nu_i$, $W^\pm l_i^\mp$, $Z\nu_i$ and $h\nu_i$ if kinematically allowed. It is shown that the branching fraction of $\psi_{3/2} \rightarrow W^\pm l_i^\mp$ is the largest [4], which means that the decay products after cascading decay of $W^\pm l_i^\mp$ are mixture of high-energy electrons/positrons, gamma rays and protons/anti-protons.⁵ Recently decaying gravitino dark matter is revised under bi-linear RPV [50, 51] to account for cosmic-ray positron excess observed in AMS-02 experiments. In our analysis we simply consider $\psi_{3/2} \rightarrow W^\pm l_i^\mp$ to avoid introducing parameters involved in determination of each branching fraction, and simulate primary and IC gamma rays. Inclusion of the other channels is straightforward (see Ref. [4]), and that will not change our result significantly.

2.2.4 Axino

Axino, a superpartner of axion originally introduced to solve the strong CP problem [52], can be dark matter in some supersymmetry models. In addition to that, if baryon number is broken by $U^c D^c D^c$ term with $\lambda''_{ijk} \lesssim 1$,⁶ baryon asymmetry is generated by moduli decay before BBN to give the observed baryon number [17]. Even in such a large RPV, it is shown that axino with a mass of $\mathcal{O}(10 \text{ GeV})$ can be long-lived to be dark matter [16].

In this model, scalar superpartners are much heavier than the electroweak scale. The interactions of axino (denoted as \tilde{a}) with squarks are then written in higher dimension operators. Ignoring down-type squarks and left-right mixing in squark sector for simplicity, it is given by

$$\mathcal{L}_{\text{int}} = \frac{\lambda''_{ijk}}{\Lambda^2} (\bar{u}_i P_L \tilde{a}) (\bar{d}_k P_L d_j^c) + \text{h.c.}, \quad (2.14)$$

where $1/\Lambda^2 = 2g_{\text{eff}}^R/m_{\tilde{u}_{R_i}}^2$. Here $m_{\tilde{u}_{R_i}}$ is supersymmetry breaking mass of \tilde{u}_{R_i} , and g_{eff}^R is one of the dimensionless couplings of axino-quark-squark interaction, which is suppressed by axino decay constant (see Refs. [12, 55]). Color indices are implicit. Then axino decays in three-body process: $\tilde{a} \rightarrow u_i d_j d_k$, $\bar{u}_i \bar{d}_j \bar{d}_k$. If quark masses are ignored, then the energy distribution of final state quarks is simply given by

$$\frac{d^2\Gamma_{\tilde{a} \rightarrow u_i d_j d_k}}{dz_i dz_j} = \frac{d^2\Gamma_{\tilde{a} \rightarrow \bar{u}_i \bar{d}_j \bar{d}_k}}{dz_i dz_j} = \frac{3|\lambda''_{ijk}|^2 m_{\tilde{a}}^5}{128\pi^3 \Lambda^4} z_i(1-z_i), \quad (2.15)$$

where $m_{\tilde{a}}$ is axino mass, $z_i = 2E_i/m_{\tilde{a}}$ and $z_j = 2E_j/m_{\tilde{a}}$ are defined by the energy E_i and E_j of u_i and d_j , respectively. Then it is straightforward to give the energy distribution of each

⁵Neutrinos are also produced, but they are irrelevant in our discussion.

⁶See Refs. [53, 54] for realization of such case.

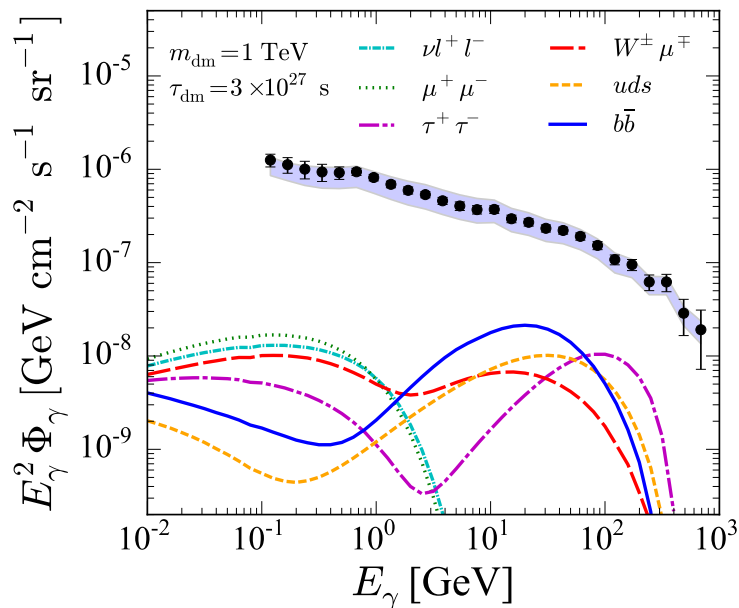


Figure 1. Gamma-ray fluxes from various decaying dark matter ($m_{\text{dm}} = 1 \text{ TeV}$, $\tau_{\text{dm}} = 3 \times 10^{27} \text{ s}$). Plots give fluxes from decay channels: (a) $\nu_e \mu^- \mu^+$ ($\bar{\nu}_e \mu^+ \mu^-$) and $\nu_\mu e^- \mu^+$ ($\bar{\nu}_\mu e^+ \mu^-$), (b) $\mu^+ \mu^-$, (c) $\tau^+ \tau^-$, (d) $W^\pm \mu^\mp$, (e) uds ($\bar{u} \bar{d} \bar{s}$), and (f) $b\bar{b}$. Data points with error bar and a band of the EGRB observed by Fermi-LAT is also shown [24] (see Sec. 3).

final state quark:

$$\frac{dN_i}{dz_i} = 12z_i^2(1 - z_i), \quad \frac{dN_j}{dz_j} = 2z_j^2(3 - 2z_j), \quad (2.16)$$

in a single process $\tilde{a} \rightarrow u_i d_j d_k$. The energy distribution for d_k is the same as d_j . These quarks are hadronized to produce mesons, which decay to gamma rays and electrons/positrons, and electrons/positrons become source of IC photons. In later numerical analysis, we also compute a case of final state $b\bar{b}$ for comparison, which would be useful for those who are interested in.

2.3 Gamma-ray fluxes (examples)

In Fig. 1 gamma-ray fluxes in various decaying dark matter models are plotted. For leptophilic case, result is shown for a case where only λ'_{122} is relevant (dubbed as “ $\nu l^+ l^-$ ”) in \tilde{W}^0 dark matter, while decay channels $\mu^+ \mu^-$ and $\tau^+ \tau^-$ are considered in $\tilde{\nu}_R$ decay. It is seen that the gamma-ray spectra from LLE^c and $\mu^+ \mu^-$ are quite similar. On the other hand, in $\tau^+ \tau^-$, the spectrum has double peaks. This is due to primary gamma rays produced from cascade decay of tau, which gives another gamma-ray flux in high energy region. For hadronically decaying dark matter, the axino decay via λ''_{122} is considered (denoted as “ uds ”). The spectrum shows similar behavior to $\tau^+ \tau^-$ case and $b\bar{b}$ channel as well. Finally, the flux from decaying gravitino to $W^\pm \mu^\mp$ is expected to have a property in the middle of leptophilic and hadrophilic cases, which is in fact seen in the figure.

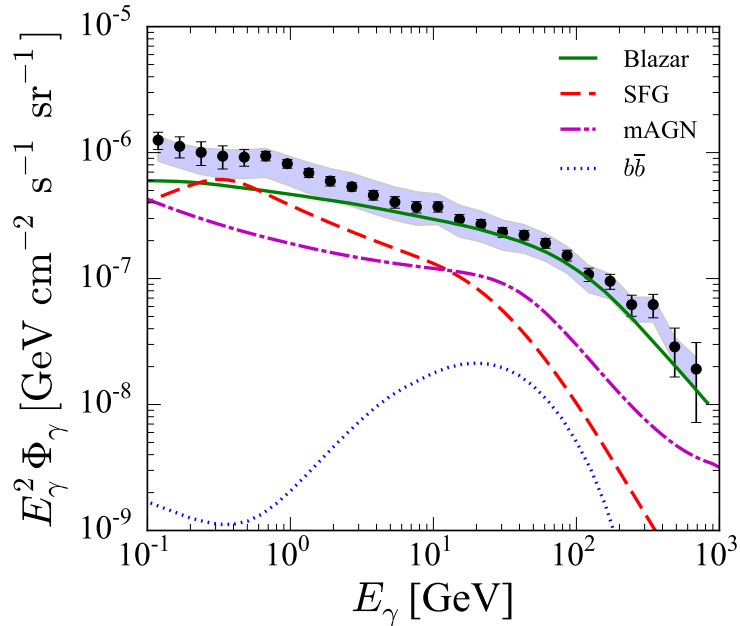


Figure 2. EGRB spectrum from blazars (solid), star-forming galaxies (dashed), misaligned active galaxies (dot-dashed), and dark matter decay (dotted; $m_{\text{dm}} = 1$ TeV, $\tau_{\text{dm}} = 3 \times 10^{27}$ s, $b\bar{b}$ decay channel). Data with error bars show the latest Fermi-LAT measurement [24], and a band attached to them show systematic uncertainty due to foreground subtraction (see Sec. 4.2). Note these data are *total* EGRB, which includes already resolved sources. *Unresolved* EGRB (or also referred to as *isotropic* gamma-ray background), on the other hand, is about a factor of two smaller [24].

3 Astrophysical source

Conventional astrophysical sources emit gamma rays through particle acceleration followed by interactions between accelerated charged particles and surrounding media or photon fields. The total EGRB should be made of both dark matter and astrophysical components:

$$\Phi_{\gamma}(E_{\gamma}) = \Phi_{\gamma}^{\text{astro}}(E_{\gamma}) + \Phi_{\gamma}^{\text{dm}}(E_{\gamma}) . \quad (3.1)$$

In this section we discuss three possible astrophysical sources in extragalactic region. They are blazars, star-forming galaxies (SFGs), and misaligned active galactic nuclei (mAGNs).

3.1 Blazars

In the GeV gamma-ray sky, the most dominant source is blazars, which are one class of active galaxies whose jets are directed towards us. More than thousand blazars have been identified with Fermi-LAT [56] and they indeed make up a significant fraction ($\sim 70\%$) of the total measured EGRB intensity [24, 35]. Therefore, it is essentially important to include this source class with a particular care.

Since many blazars have been identified with known redshifts, it is possible to reconstruct its gamma-ray luminosity function (i.e., number density of blazars per unit luminosity range). This has been done extensively, and thus far, the luminosity-dependent density evolution model that is motivated by possible underlying correlations between X-ray and

gamma-ray luminosities gives the most reasonable fit to both the luminosity and redshift distributions. The luminosity functions constructed this way can be found in Refs. [57, 58] for flat-spectrum radio quasars and BL Lactae objects, respectively (each is a subclass of the blazar population). In this study, we adopt the EGRB spectrum due to blazar population from Ref. [35] based on the latest reconstruction of the blazar luminosity function, which is shown in Fig. 2. The current uncertainty range of the spectrum is about $\sim 30\%$, almost independent of energy. Fig. 2 shows that the blazars makes up of significant fraction of the EGRB. This is not very surprising because the EGRB data shown in the figure also includes all the resolved extragalactic sources, most of which are blazars. However, it is quite clear that they cannot be the *only* source that can explain the EGRB in the entire energy region between 100 MeV and 820 GeV.

3.2 Star-forming galaxies

SFGs are galaxies that are undergoing active star formation just like our own Milky-Way Galaxy. Even though they are in general much dimmer than the blazars, already several of them are detected with Fermi-LAT [59]. The same study also found a tight correlation between the gamma-ray luminosity and infrared luminosity for these identified galaxies. Assuming that this relation universally holds and by using the precise infrared luminosity function of SFGs, one is able to construct the gamma-ray luminosity function of SFGs. Reference [60] computed the EGRB intensity due to SFGs, starburst galaxies, and SFGs containing AGNs separately, by adopting the latest infrared luminosity function constructed with the Herschel telescope [61]. The same paper found that the uncertainty of the EGRB spectrum came mainly from those due to gamma-ray-infrared luminosity correlation, and it yielded about $\sim 60\%$ uncertainties. It also yielded larger flux than the previous model [59]. Fig. 2 shows the SFG contribution (that also includes contributions from starbursts and SFGs containing AGNs). The peak around $\sim 0.3\text{--}0.5$ GeV comes from kinematical argument of the pion decay that is produced in the interactions between cosmic rays and interstellar medium. The spectrum becomes suppressed above ~ 20 GeV because of the effect of gamma-ray absorption due to the extragalactic background light. The SFG spectrum nicely complements that of blazars especially at low energies.

3.3 Misaligned active galactic nuclei

Yet another population, although much less certain, is the mAGNs, whose jets are not directed towards the Earth. (They are also known as radio galaxies.) Even though they are less bright than the blazars in gamma rays, a few of them are identified with Fermi-LAT. The gamma-ray luminosity function for this population is constructed with the radio luminosity function and measured correlation between radio and gamma-ray luminosities. Although with much larger uncertainties, this has been done in the literature [62, 63], and for this work, we adopt the model of Ref. [62] that is also shown in Fig. 2. The uncertainty is still quite large due to paucity of the detected sources, which is typically a factor of three.

4 Results

We give the lower bound for the lifetime of dark matter. Based on the discussion in Sec. 2, we consider following final state in dark matter decay; $\nu_e\mu^-\mu^+$ ($\bar{\nu}_e\mu^+\mu^-$) & $\nu_\mu e^-\mu^+$ ($\bar{\nu}_\mu e^+\mu^-$), $\mu^+\mu^-$, $\tau^+\tau^-$, $W^\pm\mu^\mp$, uds ($\bar{u}\bar{d}\bar{s}$), $b\bar{b}$.

Table 1. Priors for dark matter and astrophysical parameters.

Prior	τ_{dm}	f_{blazar}	f_{SFG}	f_{mAGN}
Normal	$20 < \log(\tau_{\text{dm}}/\text{s}) < 30$	$\sigma_{\log f} = 0.1$	$\sigma_{\log f} = 0.2$	$\sigma_{\log f} = 0.5$
Flat	$20 < \log(\tau_{\text{dm}}/\text{s}) < 30$	$-5 < \log f < 2$	$-5 < \log f < 2$	$-5 < \log f < 2$

4.1 Analysis

With the EGRB data measured with Fermi-LAT [24] and both the dark matter and astrophysical models discussed in the previous sections, we perform the Bayesian statistical analysis using the Markov-Chain Monte Carlo simulation to obtain 95% credible lower limit on dark matter decay lifetime for given dark matter model characterized by mass and decay channel.

The posterior probability distribution of parameters $\boldsymbol{\vartheta}$ given data \mathbf{d} , $P(\boldsymbol{\vartheta}|\mathbf{d})$, is related to the prior $P(\boldsymbol{\vartheta})$ and the likelihood function $\mathcal{L}(\mathbf{d}|\boldsymbol{\vartheta})$ through

$$P(\boldsymbol{\vartheta}|\mathbf{d}) \propto P(\boldsymbol{\vartheta})\mathcal{L}(\mathbf{d}|\boldsymbol{\vartheta}) . \quad (4.1)$$

We assume that the likelihood function $\mathcal{L}(\mathbf{d}|\boldsymbol{\vartheta})$ is approximated to be normal distribution

$$\mathcal{L}(\mathbf{d}|\boldsymbol{\vartheta}) = \prod_i \frac{1}{\sqrt{2\pi}\sigma_{\Phi_i}} \exp\left(-\frac{[\Phi_i - \Phi_{\gamma}^{\text{dm}}(E_i|\tau_{\text{dm}}) - \Phi_{\gamma}^{\text{astro}}(E_i|f_{\text{blazar}}, f_{\text{SFG}}, f_{\text{mAGN}})]^2}{2\sigma_{\Phi_i}^2}\right) , \quad (4.2)$$

where E_i and Φ_i represent the energy and the EGRB intensity data in i -th bin, respectively. The 1σ errors for Φ_i , assumed to be uncorrelated between different energy bins, are shown as σ_{Φ_i} (and also as the error bars in Fig. 2). For theoretical parameters, we adopt the dark matter lifetime, τ_{dm} , and energy-independent normalization for each of the astrophysical components, f_{blazar} , f_{SFG} , and f_{mAGN} , for which $f = 1$ recovers our reference spectra shown in Fig. 2.

For the prior $P(\tau_{\text{dm}})$, we adopt a flat distribution in $\log \tau_{\text{dm}}$ in the range of $20 < \log(\tau_{\text{dm}}/\text{s}) < 30$, which covers quite a wide range without any bias. Regarding the prior for the astrophysical parameters, we adopt normal distributions centered on $\log f = 0$, and with standard deviation of $\sigma_{\log f_{\text{blazar}}} = 0.1$, $\sigma_{\log f_{\text{SFG}}} = 0.2$, and $\sigma_{\log f_{\text{mAGN}}} = 0.5$, based on the errors 25%, 60%, and 200%, for the blazars, SFGs, and mAGNs, respectively. Although the errors of blazar depend on the energies of gamma ray, they are $\sim 25\%$ in most energy bins, while they are larger ($\sim 30\%$) at a few high-energy bins. These ‘Normal’ priors, also summarized Table 1, accommodate the best knowledge thus far obtained for the astrophysical sources as discussed in Sec. 3. We note that since the information of the resolved sources are already used in order to obtain these Normal priors, here we adopt the errors on *unresolved* EGRB intensity [24] in denominator of Eq. (4.2). For the gamma-ray intensity, on the other hand, we use the data of the total EGRB.

In order to give more conservative limits, we also discuss the case without any astrophysical prior information, for which we simply adopt the log-flat priors for all f parameters, between $-5 < \log f < 2$. These ‘Flat’ priors are summarized in Table 1. Since f parameters follow the log-flat distribution down to a very small value ($f = 10^{-5}$), the parameter space includes a case where the astrophysical sources give virtually zero contribution. Thus, in order to analyze consistently, we adopt the data Φ_i and errors σ_{Φ_i} for the unresolved EGRB

Table 2. Priors for phenomenological parameters for ‘astrophysical’ component.

Prior	f_{PL}	γ	E_{cut}
PL	$-2 < \log f < 2$	$-3.5 < \gamma < -1$	$100 < E_{\text{cut}}/\text{GeV} < 600$

(see caption of Fig. 2). We note that this approach is somewhat pessimistic, because many astrophysical sources are known to give contributions to the unresolved part of the EGRB, and hence taking extremely small values for f will result in significant underestimate of these astrophysical components.

For purely phenomenological purpose and also in comparison to the results with 10-month Fermi data in the literature [32], we also adopt a single cutoff power-law component for non dark matter EGRB. Although from Fig. 2 such a single cutoff power-law model appears to give reasonable fit to the Fermi data (indeed it does [24]), it is no longer strongly motivated since the resolved components (mainly blazars) are already shown to feature quite different spectral shape than the EGRB data. For this phenomenological power-law model (labeled as ‘PL’), we adopt the normalization factor f_{PL} , where $f_{\text{PL}} = 1$ corresponds to the best fit parameter to the data on its own, the spectral index γ , and the exponential cutoff energy E_{cut} , following Ref. [24]. For f_{PL} , we use the log-flat prior, and for the other two flat priors in linear scale. The ranges of these priors are summarized in Table 2.

4.2 Constraints on dark matter lifetime

Figure 3 shows 95% credible lower limits on the decay lifetime as function of its mass for various decay channels. Here we adopted the astrophysical background models with Normal prior (Table 1), which should be regarded as our canonical results based on our most up-to-date knowledge on astrophysical sources. Thick solid curves in Fig. 3 shows the lifetime constraints obtained with the data shown in Fig. 2. These data are obtained after the Galactic foreground emission being subtracted, after it was modeled with a parameter set of the Galactic cosmic ray propagation (model A in Ref. [24].) We find that the new lifetime constraints are much more stringent than those obtained with the 10-month data by up to more than one order of magnitude.

In leptonically decaying dark matter models, such as $\mu^+\mu^-$ and $\nu_e\mu^-\mu^+$ ($\bar{\nu}_e\mu^+\mu^-$) & $\nu_\mu e^-\mu^+$ ($\bar{\nu}_\mu e^+\mu^-$), constraint on the lifetime becomes stringent almost monotonically as m_{dm} and $\tau_{\text{dm}} < 10^{27}\text{--}10^{28}$ s around $m_{\text{dm}} \sim 10$ TeV is excluded. This can be understood since gamma rays in IC process is the only contribution from dark matter and the peak of the intensity (i.e. $E_\gamma^2\Phi_\gamma^{\text{dm}}$) shifts to the region where Fermi-LAT data have better accuracy as m_{dm} increases. (See Fig. 1.) In the other cases, where decay products contain lots of hadrons, the lifetime shorter than 10^{28} s is almost excluded for dark matter masses between a few 100 GeV and ~ 1 TeV. As opposed to the leptophilic case, the constraints get weaker for $m_{\text{dm}} \gtrsim 1$ TeV. This is because the gamma-ray spectrum have two peaks which comes from the cascade decay and one from IC process. When $m_{\text{dm}} \gtrsim \text{TeV}$, a ‘valley’ in the spectrum enters in the range $1 \text{ GeV} \lesssim E_\gamma \lesssim 100 \text{ GeV}$, where Fermi-LAT data is given with small errors. Thus the constraint gets relaxed.⁷

Quantitative arguments depend on the foreground model adopted and subtracted from the total gamma-ray emission. To this end, we repeated the same computation by using two

⁷Those interpretation is qualitative. Quantitative behavior is determined by non-trivial interplay between modeling of the foreground subtraction and choices of the prior. See discussion below.

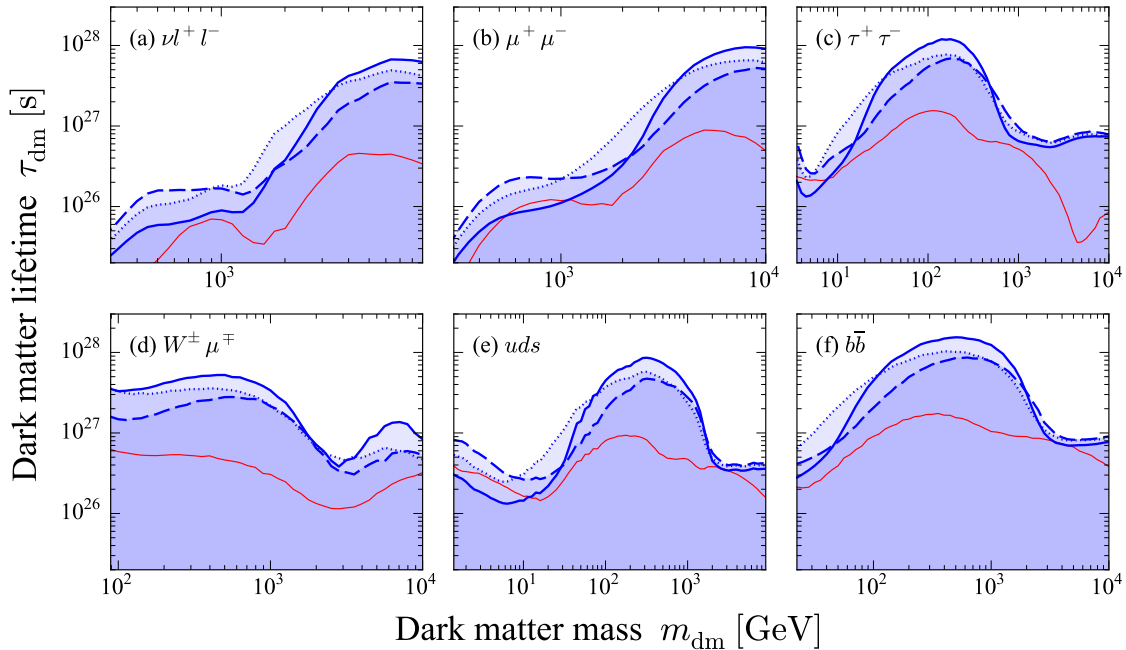


Figure 3. 95% credible lower limits on dark matter lifetime τ_{dm} as function of dark matter mass m_{dm} , for decay channels: (a) $\nu_e \mu^- \mu^+$ ($\bar{\nu}_e \mu^+ \mu^-$) and $\nu_\mu e^- \mu^+$ ($\bar{\nu}_\mu e^+ \mu^-$), (b) $\mu^+ \mu^-$, (c) $\tau^+ \tau^-$, (d) $W^\pm \mu^\mp$, (e) uds ($\bar{u}\bar{d}\bar{s}$), (f) $b\bar{b}$. Astrophysical background models with Normal priors are adopted (Table 1). Thick solid, dashed, and dotted curves correspond to the EGRB data with different foreground modeling discussed in Ref. [24] (their models A, B, and C, respectively). Thin solid curve shows the lower limits obtained with the 10-month Fermi-LAT data [34] and the phenomenological power-law background modeling.

different foreground models, B and C adopted also in Ref. [24]. Models A–C nicely covers regions shown as uncertainty band in Fig. 2. The dashed and dotted curves are the results corresponding to models B and C, respectively. This shows that the foreground modelings give uncertainty on lifetime constraints by about a factor of a few.

The results of more conservative approach with Flat priors in Table 1 are shown in Fig. 4. As expected, in most cases, they are weaker than the ones with Normal priors (as shown in Fig. 3) by about a factor of a few. Exceptions are at high dark matter masses for (c)–(f), where they give stronger constraints; this is likely caused by interplay between different choices of priors and the data (the total EGRB data for the Normal priors, while the unresolved EGRB data for the Flat priors).

In order to compare our results with the previous ones in the literature (e.g., Ref. [32]), we also computed the lifetime constraints by using the 10-month Fermi-LAT data [34]. Here we modeled the other background component as a single power law (Table 2), and the results are shown as a thin curve in each panel of Figs. 3, 4 and 5 for reference. Although the statistics adopted here is different than that in Ref. [32] (Bayesian versus frequentist), our results are in good agreement with theirs, proving the consistency of both the approaches.⁸

⁸The result for $\tau^+ \tau^-$ in high mass region is different from Ref. [32]. This is because they used both published and preliminary data for $E_\gamma > 100$ GeV (at that time) while we use the published 10-month data only. In $\tau^+ \tau^-$ case, gamma-ray spectrum from cascade decay is hard and the peak of the intensity is out of

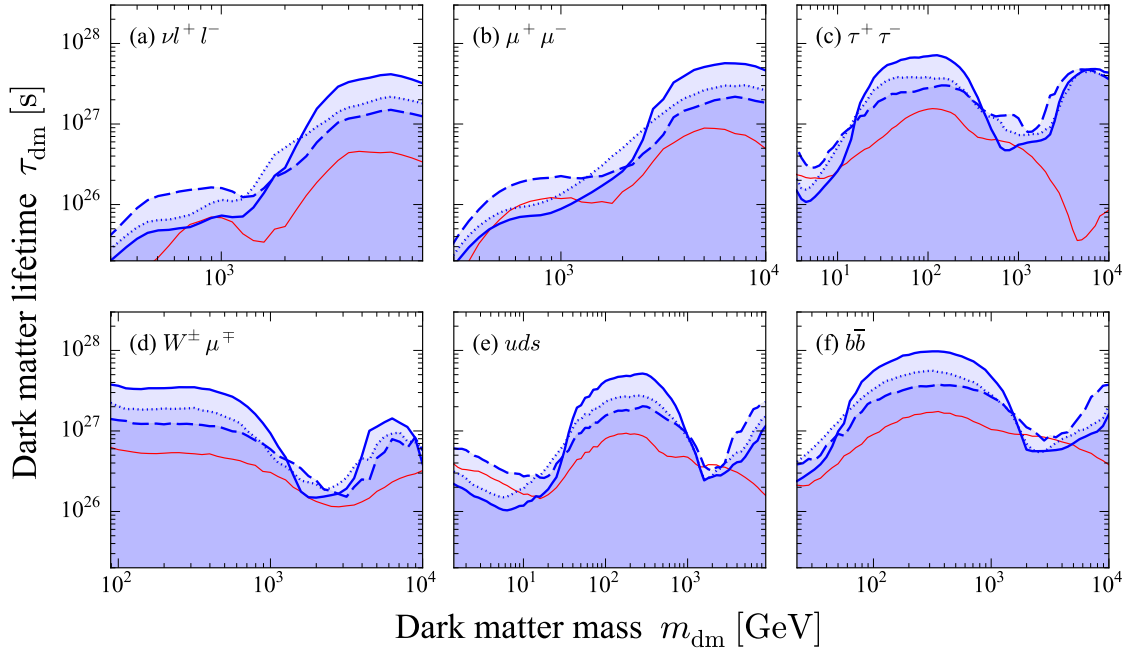


Figure 4. The same as Fig. 3, but for the astrophysical background models with Flat priors (Table 1). Note that these priors are very conservative.

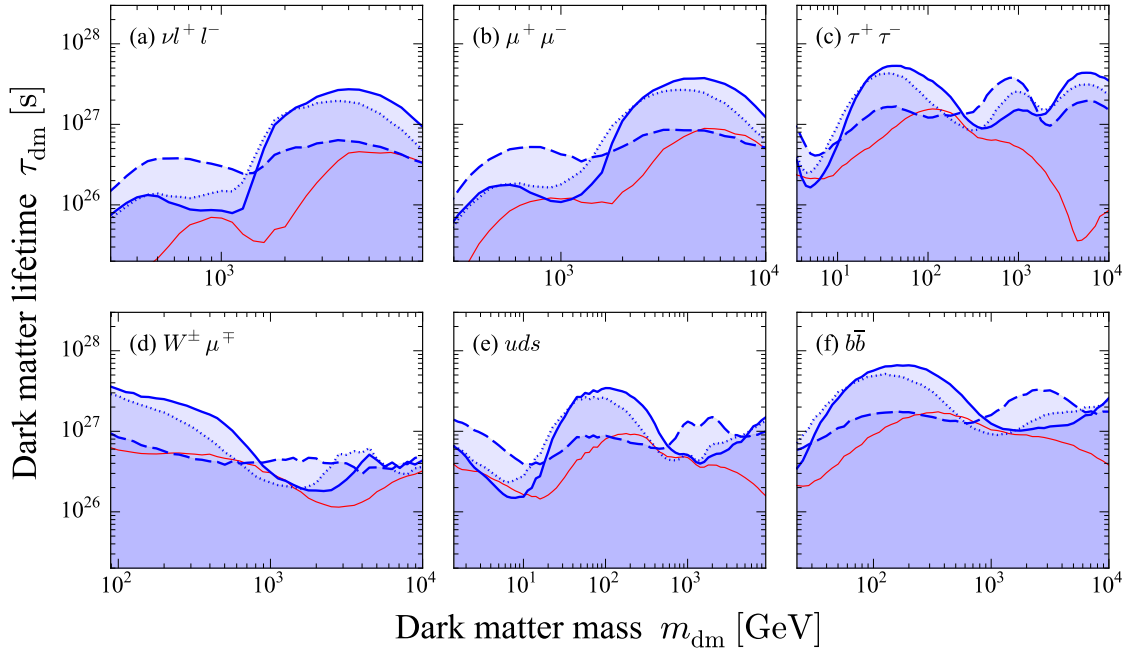


Figure 5. The same as Fig. 3, but for phenomenological background models with PL prior (Table 2).

data region when $m_{\text{dm}} \gtrsim \text{TeV}$. Then the constraint becomes weaker.

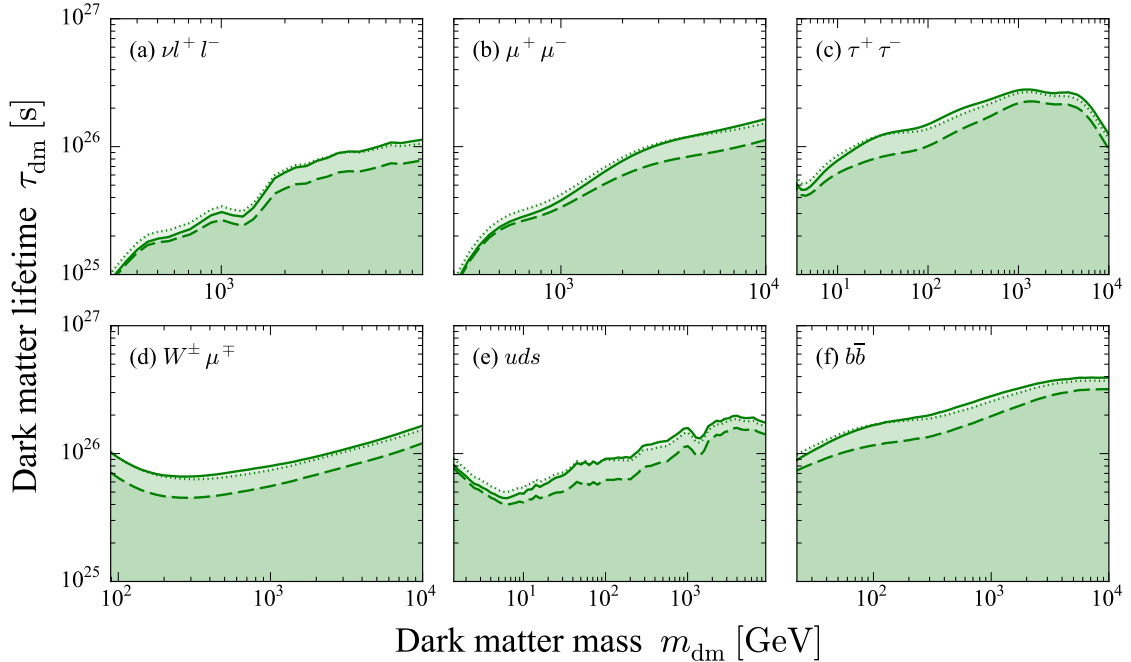


Figure 6. The same as Fig. 3, but taking into account only dark matter contribution.

In Fig. 5, we show results by using the phenomenological cutoff power-law model as the astrophysical component. Again, this is just for reference purpose, since such a single-component astrophysical modeling is no longer valid.

Finally in Fig. 6 we repeated our analysis by switching off all astrophysical components, i.e. taking into account only dark matter component, for reference. This result corresponds to the most conservative limit on the lifetime, which may be helpful for some readers.

4.3 Implications for particle physics models

As discussed, dark matter models in which large amount of high-energy electrons and positrons are produced are phenomenologically motivated in order to explain the observed cosmic-ray positron excess. Typically a lifetime of 10^{26} s with a mass of ~ 1 TeV is required to account for the excess. Our result indicates that such dark matter models are almost excluded already.

The parameter region of decaying gravitino via LH_u RPV, $m_{3/2} = 1\text{--}2$ TeV and $\tau_{3/2} \simeq 10^{26}$ s [51] to explain the latest AMS-02 positron data, is excluded in both Normal and Flat priors (Figs. 3 and 4). In Ref. [51] constraint from the EGRB is also discussed. Taking into account the astrophysical sources and 50-month Fermi-LAT data, they concluded that the decaying gravitino with the positron excess-motivated region is not excluded, which is inconsistent with our result.⁹ The decay channel $\mu^+\mu^-$ to explain the positron excess is excluded as well. The same conclusion is already stated by Ref. [32]. We have confirmed their conclusion in more sophisticated treatment for astrophysical sources. Lastly decaying

⁹This statement was based on the first version of Ref. [51]. In the second version they fixed a bug in the computation of gamma-ray flux and gave a consistent result with ours. We thank German Gomez-Vargas for pointing this out.

wino dark matter via LLE^c interaction to give sufficient positron flux to explain AMS-02 data is also excluded for thermal wino with a mass of 3 TeV.

The lifetime of dark matter which decays mainly through $U^c D^c D^c$ RPV is severely constrained too. In such case, though decaying dark matter no longer explains the positron excess, decaying axino, for instance, with a mass of $\mathcal{O}(10 \text{ GeV})$ is motivated in the context of baryogenesis, which has been mentioned in the previous sections. The results obtained in this study shows that $\tau_{\tilde{a}} = 10^{26} - 10^{27} \text{ s}$ for $\mathcal{O}(10 \text{ GeV})$ axino mass are partly excluded. This means that the parameter space of axino dark matter in moduli-induced baryogenesis may be probed in the future observation.

Here we have discussed the implication of our numerical results for the dark matter models described in Sec. 2.2. However, it is obvious that the results given in Sec. 4.2 does not depend on what dark matter is. Only the decay products of dark matter, i.e. the final state, change the constraints on the lifetime of dark matter (as function of its mass). Thus, if gravitino decays via LLE^c RPV, for example, then the result of (a) in Figs. 3 and 4 can be roughly applied.¹⁰

5 Discussion

5.1 Comparison with constraints from galaxy clusters and dwarf galaxies

There are other regions of the sky that can be used to constrain dark matter decay through gamma rays. The largest virialized dark matter structures, known as clusters of galaxies, were studied in the literature for the purpose [64, 65]. Dwarf spheroidal galaxies are nearby dark matter substructure in the Galaxy that are highly dark matter dominated, and hence they are considered ideal for dark matter searches. The dwarf galaxies were also studied for constraining dark matter decay [64]. Here, we compare them with the EGRB that was used in our study.

Gamma-ray intensity Φ_γ is proportional to line-of-sight integral of dark matter density as was discussed in Sec. 2.1. In case of the EGRB where the integration should be taken up to the Hubble horizon, this quantity is

$$J_{\text{EGRB}} = \frac{c\Omega_{\text{dm}}\rho_c}{H_0} \int dz \frac{1}{\sqrt{\Omega_\Lambda + \Omega_m(1+z)^3}}, \quad (5.1)$$

and is $3 \times 10^{22} \text{ GeV cm}^{-2}$ if we integrate over $0 < z < 5$. Note that we here ignored gamma-ray absorption as well as the gamma-ray spectrum per decay dN_γ/dE found in Eq. (2.7), in order to have order-of-magnitude insight of the relevant term. This is now compared with the same quantity for the galaxy clusters and dwarf galaxies, after smeared over the Fermi-LAT angular resolution. Reference [64] computed it for both the sources, and found that they were typically $2 \times 10^{22} \text{ GeV cm}^{-2}$ for the most promising cluster (Fornax) and more than one order of magnitude smaller for all the known dwarf galaxies, after averaging over the region with 1° radius. They are not only smaller than J_{EGRB} but also subject to uncertainties on dark matter density profiles. In addition, the EGRB spectrum is inferred from the all-sky data, where there are many more photons available for the analysis than small regions around galaxy clusters or dwarf galaxies. Therefore, we conclude that the EGRB provides the best opportunity to constrain dark matter decay with gamma rays.

¹⁰Strictly speaking, the energy distribution of charged leptons from gravitino decaying in three body are different. However, the difference will not change the constraints on the lifetime significantly.

5.2 Comparison with constraints from Galactic anti-protons

If dark matter decays hadronically, it produces lots of protons and anti-protons. Since high-energy anti-protons are rare in canonical Galactic activities, measurements of cosmic-ray anti-proton constrain hadronic decay of dark matter. However, it is known that there is huge theoretical uncertainty in the calculation of cosmic-ray anti-proton in the Galactic region. Cosmic-ray anti-proton flux can be calculated in a Galactic propagation model, which has several parameters. They are determined by using the measurements of other cosmic rays, such as proton flux and boron-to-carbon ratio, etc., which unfortunately cannot determine all of the parameters. Propagation models called ‘MAX’, ‘MED’ and ‘MIN’ are the typical examples [66]. Although they are consistent with the measurements of other light elements in cosmic rays, they give different predictions for anti-proton flux. In decaying dark matter model, the anti-proton flux changes up to an order of magnitude between MAX and MIN models (see Ref. [28], for example).¹¹ In addition, the constraint becomes much weaker in low dark matter mass region, i.e. $m_{\text{dm}} \lesssim 100$ GeV [28]. On the contrary, the constraints from the EGRB we have studied in this paper have less uncertainty compared to those in cosmic ray \bar{p} . It is noticed that there also exists an uncertainty which is involved in Galactic propagation model. The 50-month data from Fermi-LAT [24] is given by using GALPROP package [69] in order to simulate diffuse gamma rays in the Galactic region. They discuss the uncertainty by computing inner-Galactic gamma rays in different Galactic models, which corresponds to models A, B, and C described in the previous sections. Our results show that the constraints on dark matter model changes within an order of magnitude in the three models. Thus observation of the EGRB gives much more robust limits on decaying dark matter model with less uncertainty compared to the limits from anti-proton flux. In addition, it should be noted that the 50-month data gives much more stringent constraint on the lifetime than 10-month data in all types of dark matter models studied here. Thus more accumulated data with expanded analyses including anisotropies [70, 71] will give probably the best limits on decaying dark matter models in the future.

6 Conclusions

We have studied the extragalactic gamma-ray background in decaying dark matter models. Decaying dark matter produces gamma rays both primarily from the cascade decay and from electron/positron through inverse Compton scattering off the microwave-background photons. If the final state, along with its mass and lifetime of decaying dark matter, is specified, the gamma-ray spectrum can be computed with little theoretical uncertainty. Astrophysical sources of gamma rays in extragalactic region, on the other hand, have been resolved with gamma-ray telescopes such as Fermi. Main components, which are blazars, star-forming galaxies and misaligned active galactic nuclei, give rise to consistent flux with the measurement of the gamma-ray background according to Fermi. We have used the updated astrophysical models for those components and the latest Fermi data after 50-month sky survey to constrain decaying dark matter models. In order to make qualitative statement for various class of models, we have considered supersymmetric dark matter in R -parity violation. Supersymmetric model accommodates variety of dark matter candidates, such as wino, gravitino, sneutrino and axino and so on. They decay to standard-model particles leptonically or hadronically, depending on the relevant R -parity violating interaction. We

¹¹See also Refs. [67, 68] for recent development.

have calculated gamma-ray flux in the models where dark matter mainly decays to $l_j^+ l_k^-$, $\nu_i e_j^- e_k^+$ ($\bar{\nu}_i e_j^+ e_k^-$), $W^\pm l_i^\mp$, $u_i d_j d_k$ ($\bar{u}_i \bar{d}_j \bar{d}_k$), and $q_i \bar{q}_i$. The numerical analysis shows that the constraints on the lifetime of dark matter becomes more stringent by a factor of a few to an order of magnitude, compared to the past work. As the result, we found that leptonically (and hadronically) decaying dark matter which explains the cosmic ray positron excess is excluded in most cases. Hadronically decaying dark matter is also severely constrained. For example, the current Fermi data are beginning to exclude part of parameter space of decaying axino dark matter in moduli-induced baryogenesis, which indicates that future observation of the extragalactic gamma ray may probe this model.

Acknowledgments

We thank Francesca Calore and Irene Tamborra for providing spectral data of mAGNs and SFGs, respectively. SA was supported by the Netherlands Organization for Scientific Research (NWO) through a Vidi grant. KI has been supported in part by the German Science Foundation (DFG) within the Collaborative Research Center 676 Particles, Strings and the Early Universe.

References

- [1] G. Hinshaw *et al.* [WMAP Collaboration], *Astrophys. J. Suppl.* **208**, 19 (2013) [arXiv:1212.5226 [astro-ph.CO]].
- [2] P. A. R. Ade *et al.* [Planck Collaboration], *Astron. Astrophys.* **571**, A16 (2014) [arXiv:1303.5076 [astro-ph.CO]].
- [3] F. Takayama and M. Yamaguchi, *Phys. Lett. B* **485**, 388 (2000) [hep-ph/0005214].
- [4] K. Ishiwata, S. Matsumoto and T. Moroi, *Phys. Rev. D* **78**, 063505 (2008) [arXiv:0805.1133 [hep-ph]].
- [5] K. Rajagopal, M. S. Turner and F. Wilczek, *Nucl. Phys. B* **358**, 447 (1991).
- [6] T. Goto and M. Yamaguchi, *Phys. Lett. B* **276**, 103 (1992).
- [7] T. Asaka and M. Yamaguchi, *Phys. Lett. B* **437**, 51 (1998) [hep-ph/9805449]; T. Asaka and M. Yamaguchi, *Phys. Rev. D* **59**, 125003 (1999) [hep-ph/9811451].
- [8] N. Abe, T. Moroi and M. Yamaguchi, *JHEP* **0201**, 010 (2002) [hep-ph/0111155].
- [9] K. Choi and K. S. Jeong, *JHEP* **0701**, 103 (2007) [hep-th/0611279].
- [10] K. Choi, K. S. Jeong, K. I. Okumura and M. Yamaguchi, *JHEP* **1106**, 049 (2011) [arXiv:1104.3274 [hep-ph]].
- [11] E. J. Chun, J. E. Kim and H. P. Nilles, *Phys. Lett. B* **287**, 123 (1992) [hep-ph/9205229]; E. J. Chun, H. B. Kim and J. E. Kim, *Phys. Rev. Lett.* **72**, 1956 (1994) [hep-ph/9305208].
- [12] L. Covi, J. E. Kim and L. Roszkowski, *Phys. Rev. Lett.* **82**, 4180 (1999) [hep-ph/9905212]; L. Covi, H. B. Kim, J. E. Kim and L. Roszkowski, *JHEP* **0105**, 033 (2001) [hep-ph/0101009]; K. -Y. Choi, L. Covi, J. E. Kim and L. Roszkowski, *JHEP* **1204**, 106 (2012) [arXiv:1108.2282 [hep-ph]].
- [13] S. Nakamura, K. i. Okumura and M. Yamaguchi, *Phys. Rev. D* **77**, 115027 (2008) [arXiv:0803.3725 [hep-ph]].
- [14] T. Banks, M. Dine and M. Graesser, *Phys. Rev. D* **68**, 075011 (2003) [hep-ph/0210256].

- [15] M. Kawasaki, K. Nakayama and M. Senami, JCAP **0803**, 009 (2008) [arXiv:0711.3083 [hep-ph]].
- [16] K. Ishiwata, JHEP **1409**, 122 (2014) [arXiv:1407.1827 [hep-ph]].
- [17] K. Ishiwata, K. S. Jeong and F. Takahashi, JHEP **1402**, 062 (2014) [arXiv:1312.0954 [hep-ph]].
- [18] C. Cheung and K. Ishiwata, Phys. Rev. D **88**, no. 1, 017901 (2013) [arXiv:1304.0468 [hep-ph]].
- [19] O. Adriani *et al.* [PAMELA Collaboration], Nature **458**, 607 (2009) [arXiv:0810.4995 [astro-ph]].
- [20] O. Adriani *et al.* [PAMELA Collaboration], Phys. Rev. Lett. **111**, no. 8, 081102 (2013) [arXiv:1308.0133 [astro-ph.HE]].
- [21] M. Ackermann *et al.* [Fermi LAT Collaboration], Phys. Rev. Lett. **108**, 011103 (2012) [arXiv:1109.0521 [astro-ph.HE]].
- [22] M. Aguilar *et al.* [AMS Collaboration], Phys. Rev. Lett. **110**, 141102 (2013).
- [23] L. Accardo *et al.* [AMS Collaboration], Phys. Rev. Lett. **113**, no. 12, 121101 (2014); M. Aguilar *et al.* [AMS Collaboration], Phys. Rev. Lett. **113**, 121102 (2014).
- [24] M. Ackermann *et al.* [The Fermi LAT Collaboration], arXiv:1410.3696 [astro-ph.HE].
- [25] K. Ishiwata, S. Matsumoto and T. Moroi, Phys. Lett. B **679**, 1 (2009) [arXiv:0905.4593 [astro-ph.CO]].
- [26] S. Profumo and T. E. Jeltema, JCAP **0907** (2009) 020 [arXiv:0906.0001 [astro-ph.CO]].
- [27] O. Adriani *et al.* [PAMELA Collaboration], Phys. Rev. Lett. **105**, 121101 (2010) [arXiv:1007.0821 [astro-ph.HE]].
- [28] M. Cirelli and G. Giesen, JCAP **1304**, 015 (2013) [arXiv:1301.7079 [hep-ph]].
- [29] M. Garny, A. Ibarra and D. Tran, JCAP **1208**, 025 (2012) [arXiv:1205.6783 [hep-ph]].
- [30] A. Ibarra and D. Tran, JCAP **0807**, 002 (2008) [arXiv:0804.4596 [astro-ph]].
- [31] K. Ishiwata, S. Matsumoto and T. Moroi, JHEP **1012**, 006 (2010) [arXiv:1008.3636 [hep-ph]].
- [32] M. Cirelli, E. Moulin, P. Panci, P. D. Serpico and A. Viana, Phys. Rev. D **86**, 083506 (2012) [arXiv:1205.5283 [astro-ph.CO]].
- [33] M. Cirelli, P. Panci and P. D. Serpico, Nucl. Phys. B **840**, 284 (2010) [arXiv:0912.0663 [astro-ph.CO]].
- [34] A. A. Abdo *et al.* [Fermi-LAT Collaboration], Phys. Rev. Lett. **104**, 101101 (2010) [arXiv:1002.3603 [astro-ph.HE]].
- [35] M. Ajello, D. Gasparrini, M. Sanchez-Conde, G. Zaharijas, M. Gustafsson, J. Cohen-Tanugi, C. D. Dermer and Y. Inoue *et al.*, arXiv:1501.05301 [astro-ph.HE].
- [36] M. Ackermann *et al.* [The Fermi LAT Collaboration], arXiv:1501.05464 [astro-ph.CO].
- [37] M. Di Mauro and F. Donato, arXiv:1501.05316 [astro-ph.HE].
- [38] R. C. Gilmore, R. S. Somerville, J. R. Primack and A. Dominguez, Mon. Not. Roy. Astron. Soc. **422**, 3189 (2012) [arXiv:1104.0671 [astro-ph.CO]].
- [39] L. Randall and R. Sundrum, Nucl. Phys. B **557**, 79 (1999) [hep-th/9810155]; G. F. Giudice, M. A. Luty, H. Murayama and R. Rattazzi, JHEP **9812**, 027 (1998) [hep-ph/9810442].
- [40] T. Moroi and L. Randall, Nucl. Phys. B **570**, 455 (2000) [hep-ph/9906527].
- [41] J. Hisano, S. Matsumoto, M. Nagai, O. Saito and M. Senami, Phys. Lett. B **646**, 34 (2007) [hep-ph/0610249].
- [42] G. Aad *et al.* [ATLAS Collaboration], Phys. Lett. B **716**, 1 (2012) [arXiv:1207.7214 [hep-ex]].

- [43] S. Chatrchyan *et al.* [CMS Collaboration], Phys. Lett. B **716**, 30 (2012) [arXiv:1207.7235 [hep-ex]].
- [44] J. Hisano, K. Ishiwata and N. Nagata, Phys. Lett. B **690**, 311 (2010) [arXiv:1004.4090 [hep-ph]]; J. Hisano, K. Ishiwata and N. Nagata, Phys. Rev. D **82**, 115007 (2010) [arXiv:1007.2601 [hep-ph]]; J. Hisano, K. Ishiwata, N. Nagata and T. Takesako, JHEP **1107**, 005 (2011) [arXiv:1104.0228 [hep-ph]]; J. Hisano, K. Ishiwata and N. Nagata, Phys. Rev. D **87**, 035020 (2013) [arXiv:1210.5985 [hep-ph]]; R. J. Hill and M. P. Solon, arXiv:1409.8290 [hep-ph].
- [45] J. Hisano, S. Matsumoto and M. M. Nojiri, Phys. Rev. Lett. **92**, 031303 (2004) [hep-ph/0307216]; J. Hisano, S. Matsumoto, M. M. Nojiri and O. Saito, Phys. Rev. D **71**, 063528 (2005) [hep-ph/0412403].
- [46] M. Ibe, S. Matsumoto, S. Shirai and T. T. Yanagida, Phys. Lett. B **741**, 134 (2014) [arXiv:1409.6920 [hep-ph]]; M. Ibe, S. Matsumoto, S. Shirai and T. T. Yanagida, JHEP **1307**, 063 (2013) [arXiv:1305.0084 [hep-ph]].
- [47] K. Ishiwata, S. Matsumoto and T. Moroi, JHEP **0905**, 110 (2009) [arXiv:0903.0242 [hep-ph]].
- [48] T. Sjostrand, S. Mrenna and P. Z. Skands, JHEP **0605**, 026 (2006) [hep-ph/0603175].
- [49] T. Asaka, K. Ishiwata and T. Moroi, Phys. Rev. D **73**, 051301 (2006) [hep-ph/0512118]; T. Asaka, K. Ishiwata and T. Moroi, Phys. Rev. D **75**, 065001 (2007) [hep-ph/0612211].
- [50] M. Ibe, S. Iwamoto, S. Matsumoto, T. Moroi and N. Yokozaki, JHEP **1308**, 029 (2013) [arXiv:1304.1483 [hep-ph]].
- [51] E. Carquin, M. A. Diaz, G. A. Gomez-Vargas, B. Panes and N. Viaux, arXiv:1501.05932 [hep-ph].
- [52] R. D. Peccei and H. R. Quinn, Phys. Rev. Lett. **38**, 1440 (1977); Phys. Rev. D **16**, 1791 (1977).
- [53] R. Barbier, C. Berat, M. Besancon, M. Chemtob, A. Deandrea, E. Dudas, P. Fayet and S. Lavignac *et al.*, Phys. Rept. **420**, 1 (2005) [hep-ph/0406039].
- [54] B. Bhattacharjee, J. L. Evans, M. Ibe, S. Matsumoto and T. T. Yanagida, Phys. Rev. D **87**, no. 11, 115002 (2013) [arXiv:1301.2336 [hep-ph]].
- [55] E. J. Chun, Phys. Rev. D **84**, 043509 (2011) [arXiv:1104.2219 [hep-ph]].
- [56] F. Acero *et al.* [The Fermi-LAT Collaboration], arXiv:1501.02003 [astro-ph.HE].
- [57] M. Ajello, M. S. Shaw, R. W. Romani, C. D. Dermer, L. Costamante, O. G. King, W. Max-Moerbeck and A. Readhead *et al.*, Astrophys. J. **751**, 108 (2012) [arXiv:1110.3787 [astro-ph.CO]].
- [58] M. Ajello, R. W. Romani, D. Gasparri, M. S. Shaw, J. Bolmer, G. Cotter, J. Finke and J. Greiner *et al.*, Astrophys. J. **780**, 73 (2014) [arXiv:1310.0006 [astro-ph.CO]].
- [59] M. Ackermann *et al.* [Fermi LAT Collaboration], Astrophys. J. **755**, 164 (2012) [arXiv:1206.1346 [astro-ph.HE]].
- [60] I. Tamborra, S. Ando and K. Murase, JCAP **1409**, no. 09, 043 (2014) [arXiv:1404.1189 [astro-ph.HE]].
- [61] C. Gruppioni, F. Pozzi, G. Rodighiero, I. Delvecchio, S. Berta, L. Pozzetti, G. Zamorani and P. Andreani *et al.*, Mon. Not. Roy. Astron. Soc. **432**, 23 (2013) [arXiv:1302.5209 [astro-ph.CO]].
- [62] M. Di Mauro, F. Calore, F. Donato, M. Ajello and L. Latronico, Astrophys. J. **780**, 161 (2014) [arXiv:1304.0908 [astro-ph.HE]].
- [63] Y. Inoue, Astrophys. J. **733**, 66 (2011) [arXiv:1103.3946 [astro-ph.HE]].
- [64] L. Dugger, T. E. Jeltema and S. Profumo, JCAP **1012**, 015 (2010) [arXiv:1009.5988 [astro-ph.HE]].

- [65] X. Huang, G. Vertongen and C. Weniger, JCAP **1201**, 042 (2012) [arXiv:1110.1529 [hep-ph]].
- [66] T. Delahaye, R. Lineros, F. Donato, N. Fornengo and P. Salati, Phys. Rev. D **77**, 063527 (2008) [arXiv:0712.2312 [astro-ph]].
- [67] M. Boudaud, M. Cirelli, G. Giesen and P. Salati, arXiv:1412.5696 [astro-ph.HE].
- [68] R. Kappl and M. W. Winkler, JCAP **1409**, no. 09, 051 (2014) [arXiv:1408.0299 [hep-ph]].
- [69] I. V. Moskalenko and A. W. Strong, Astrophys. J. **493**, 694 (1998) [astro-ph/9710124].
A. W. Strong and I. V. Moskalenko, Astrophys. J. **509**, 212 (1998) [astro-ph/9807150];
A. W. Strong, I. V. Moskalenko and O. Reimer, Astrophys. J. **537**, 763 (2000) [Erratum-ibid. **541**, 1109 (2000)] [astro-ph/9811296]; GALPROP Homepage, <http://galprop.stanford.edu/>.
- [70] S. Ando and E. Komatsu, Phys. Rev. D **87**, no. 12, 123539 (2013) [arXiv:1301.5901 [astro-ph.CO]]; S. Ando, A. Benoit-Lvy and E. Komatsu, Phys. Rev. D **90**, no. 2, 023514 (2014) [arXiv:1312.4403 [astro-ph.CO]].
- [71] S. Camera, M. Fornasa, N. Fornengo and M. Regis, Astrophys. J. **771**, L5 (2013) [arXiv:1212.5018 [astro-ph.CO]].